Polarization Control of Linear Dipole Radiation Using an Optical Nanofiber

Maxime Joos, Chengjie Ding, Vivien Loo, Guillaume Blanquer, Elisabeth Giacobino, Alberto Bramati, Valentina Krachmalnicoff, Quentin Glorieux

Polarization Control of Linear Dipole Radiation Using an Optical Nanofiber

Maxime Joos,[1,*] Chengjie Ding,[1,2,*] Vivien Loo,[1,3] Guillaume Blanquer,[3] Elisabeth Giacobino,[1] Alberto Bramati,[1] Valentina Krachmalnicoff,[3] and Quentin Glorieux[1,†]

[1] *Laboratoire Kastler Brossel, Sorbonne Université, CNRS, ENS-PSL Research University, Collège de France*
[2] *State Key Laboratory of Precision Spectroscopy, East China Normal University, Shanghai 200062, China*
[3] *ESPCI Paris, PSL Research University, CNRS, Institut Langevin*

(Dated: December 5, 2018)

We experimentally demonstrate that a linear dipole is not restricted to emit linearly polarized light, provided it is embedded in the appropriate nanophotonic environment. We observe emission of various elliptical polarizations by a linear dipole including circularly polarized light, without the need for birefringent components. We further show that the emitted state of polarization can theoretically span the entire Poincaré sphere. The experimental demonstration is based on elongated gold nanoparticles (nanorods) deposited on an optical nanofiber and excited by a free-space laser beam. The light directly collected in the guided mode of the nanofiber is analyzed in regard to the azimuthal position and orientation of the nanorods, observed by means of scanning electron microscopy. This work constitutes a demonstration of the mapping between purely geometrical degrees of freedom of a light source and all polarization states and could open the way to new methods for polarization control of light sources at the nanoscale.

* Contributed equally to this work.
† Corresponding author: quentin.glorieux@lkb.upmc.fr

I. INTRODUCTION

The wave nature of light implies that radiation phenomena are the combined manifestation of a source and its environment. Thus, properties of light sources such as power, frequency, or directivity can be tuned by confining the source in an appropriate environment. Nanophotonics aims at controlling these properties using the interaction with wavelength-scaled structures [1] such as cavities, antennas [2] or waveguides [3]. These structures rely on the discretization of the optical modes when the spatial confinement is of the order of the wavelength but until recently, they did not explicitly make use of the vectorial nature of light. In the last decade, exploiting the strong confinement of vectorial fields has proven to be a very rich aspect of nanophotonics. Indeed, the sharp transverse confinement of vectorial fields breaks the symmetry of the intensity profile and modifies the polarization structure of the light [4]. When the transverse electric field varies significantly over a wavelength – as it is the case in evanescent waves – a longitudinal field component emerges and oscillates in phase quadrature with the transverse field. The local polarization becomes dependent on the propagation direction of light, an effect referred to as spin-momentum or polarization-direction locking of light [5] [6]. In this context, directional emission [7–9], non-reciprocal light-matter interaction [10] and developments in nano-polarization devices have been achieved [11, 12].

Optical nanofibers are privileged interfaces to investigate the interaction of spin-momentum locked light with matter. In such cylindrical waveguides, the light extends outside the fiber in the form of an evanescent field and enables easy interfacing with emitters such as atoms, quantum dots [13] or plasmonic scatterers [14].

In this work, we exploit the strong confinement of light in optical nanofibers to demonstrate that a linear (1D) dipole can emit elliptically polarized light in the transverse plane when coupled to spin-momentum locked modes. We study how the guided light polarization depends on the local orientation and position of the dipole and further show that the whole Poincaré sphere is accessible with this nanophotonics system. For example, we observed emission of quasi-circularly polarized light by a linear dipole oriented at 46° with respect to the propagation direction of light. We remark that this effect does not involve any birefringent component. This system constitutes a step toward a complete control of light emission at the nanoscale.

II. EXPERIMENTAL SYSTEM

A. Setup

Our experimental physical system is composed of a single gold nanorod deposited on the surface of an air-clad optical nanofiber as shown in figure 1a. A linearly polarized, focused laser beam illuminates the nanorod particle that behaves as a linear dipole scatterer. The polarization of the light collected in the guided mode of the nanofiber is analyzed as a function of the position of the nanorod on the fiber and of its orientation, which are measured by means of a Scanning Electron Microscope (SEM).

We use optical nanofibers produced by a standard heat-and-pull process (see [15]) in order to locally stretch a commercial single-mode fiber to a subwavelength-diameter of around 300 nm while maintaining over 95% optical transmission. At our working wavelength of 637 nm, the nanofiber only guides the fundamental mode $\mathbf{HE}_{11}$ studied in [4].

B. Model

We now consider in more detail how an electric dipole moment couples to the fundamental mode of the nanofiber. The dipole is assumed to lie flat on the nanofiber surface at an azimuthal position denoted by the angle α and forms an angle θ with respect to the propagation axis z. We use a coordinate system $(x'y'z)$ such that the dipole is located on the y'-axis, i.e at $x' = 0$. The x' and y' axes are obtained by rotation of axes x and y by an angle α around the z-axis (see figure 1). We will express the guided electric field $\mathbf{E}_g$ emitted by the dipole as a linear combination of the quasi-linearly polarized hybrid modes envelopes [4, 16]:

$$\begin{aligned} \mathbf{HE}_{11,x'} &= \mathbf{e}_{x'}(r,\varphi) + i\mathbf{e}_z(r)\cos\varphi, \\ \mathbf{HE}_{11,y'} &= \mathbf{e}_{y'}(r,\varphi) + i\mathbf{e}_z(r)\sin\varphi \end{aligned} \tag{1}$$

where r and φ are the polar coordinates in the $x'y'-$plane, $\mathbf{e}_{x'}(r,\varphi)$, $\mathbf{e}_{y'}(r,\varphi)$ are the real-valued transverse components and $\mathbf{e}_z(r)\cos\varphi$, $\mathbf{e}_z(r)\sin\varphi$ are the longitudinal components of the guided modes with main polarization along x' and y' respectively (see Appendix A for details). The guided field can then be expressed as:

$$\mathbf{E}_g = \left[A\ \mathbf{HE}_{11,x'} + B\ \mathbf{HE}_{11,y'}\right] e^{i(\beta z - \omega t)} \tag{2}$$

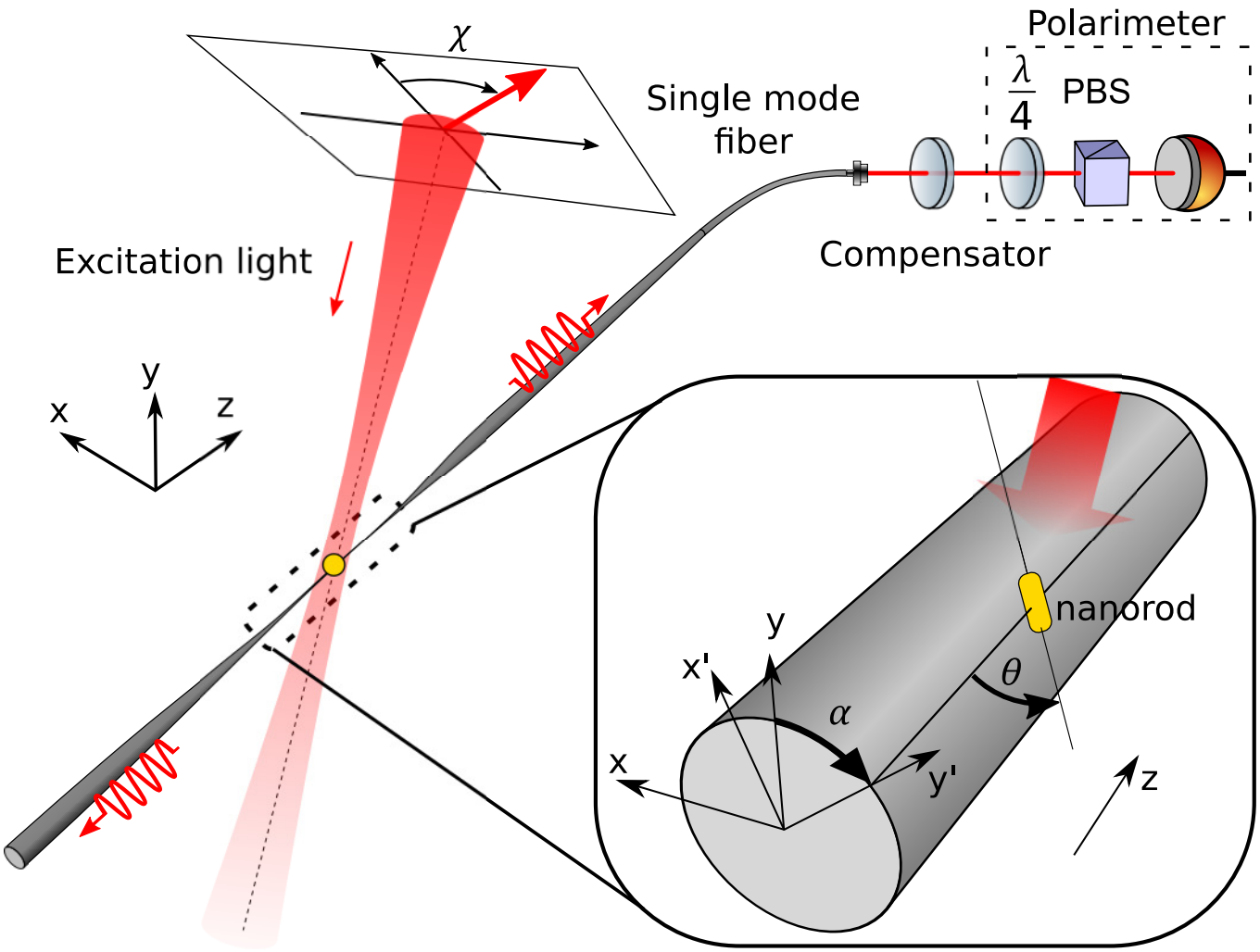

FIG. 1. **Experimental setup**. A single gold nanorod is deposited on the surface of an optical nanofiber. A focused laser beam contained in the yz-plane illuminates the particle that scatters light in the fundamental mode of the nanofiber. The nanorod lies in a plane tangent to the nanofiber surface. The normal to this plane (y') makes an angle α with the vertical (y) axis. In this plane the nanorod forms an angle θ with the nanofiber (z) direction. The guided light is then analyzed with a polarimeter allowing to measure Stokes parameters.

where β is the propagation constant and ω the angular frequency of the light field. A and B are complex coefficients determined by the projection of the dipole moment amplitude $\mathbf{d}$ onto the complex envelope of the hybrid modes (1) evaluated at the dipole position ($r = a, \varphi = \pi/2$) [8, 17], where a is the nanofiber radius: $A = \mathbf{d}^* \cdot \mathbf{HE}_{11,x'}(a, \pi/2)$ and $B = \mathbf{d}^* \cdot \mathbf{HE}_{11,y'}(a, \pi/2)$. For a linear dipole expressed in the (x', y', z) coordinate system, $\mathbf{d}$ is proportional to $(\sin\theta, 0, \cos\theta)$. It follows that $A = \mathbf{d} \cdot \mathbf{e}_{x'}(a, \pi/2)$ reduces to a single real term and $B = \mathbf{d} \cdot [\mathbf{e}_{y'}(a, \pi/2) + i\mathbf{e}_z(a)]$ reduces to a purely imaginary term since $\mathbf{e}_{y'}(a, \pi/2)$ has no x'-component and $\mathbf{d}$ no y'-component, leading to the electric field:

$$\mathbf{E}_g = [C \sin\theta \; \mathbf{HE}_{11,x'} + i \; D \cos\theta \; \mathbf{HE}_{11,y'}] \, e^{i(\beta z - \omega t)} \tag{3}$$

where C and D are real (see Appendix B). One first consequence of the coupling of the dipole to the nanofiber is that, whatever the orientation θ of the dipole, the guided field (3) never vanishes. When aligned along the nanofiber ($\theta = 0°$), the dipole can even radiate light in its axis direction –thanks to the nanofiber guided modes– in strong contrast to the dipole radiation pattern in free-space. Considering now the emitted polarization in the nanofiber: the terms of the right-hand side of (3) oscillate in phase quadrature and give rise in general, to elliptical polarization in the transverse plane. This can be understood as follow: the dipole has non-zero overlap only with the longitudinal z-component of $\mathbf{HE}_{11,y'}$ and with the transverse x'-component of $\mathbf{HE}_{11,x'}$. The dipole excites $\mathbf{HE}_{11,y'}$ through its longitudinal component and $\mathbf{HE}_{11,x'}$ through its (transverse) x'-component. For spin-momentum locked light however,

transverse and longitudinal components are in phase quadrature so that the hybrid modes $\mathbf{HE}_{11,x'}$ and $\mathbf{HE}_{11,y'}$ will also oscillate in phase quadrature.

Let us now illustrate this mechanism with two cases: when the dipole is aligned ($\theta = 0°$) or perpendicular ($\theta = 90°$) to the nanofiber. For $\theta = 0°$, the electric field (3) of the guided light reduces to $\mathbf{E}_g \propto \mathbf{HE}_{11,y'}$ which corresponds to quasi-linearly polarized light along y'. For $\theta = 90°$, light is quasi-linearly polarized along x'. Between this two limiting cases, the continuous range of polarization ellipses with axes along x' and y' is accessible. A remarkable intermediate dipole orientation, for which $|A| = |B|$ gives rise to *quasi-circularly* polarized light. This can be numerically solved and leads to $\theta_{circ} = \pm 43°$ for typical experimental conditions and a nanofiber diameter of 305 nm. The dipole orientation hence defines the ellipticity of the guided light.

The azimuth α of the dipole on the other hand determines the major axis direction of the polarization ellipse. This can be easily seen considering the situation $\theta = 0°$. As already mentioned, the guided light polarization is quasi-linear along the y' direction which is, by definition, the azimuth of the dipole.

Hence, all polarization states are deterministically accessible through the following mapping: the nanorod azimuthal position $\alpha \in [-90°, 90°]$ determines the polarization ellipse orientation ψ or equivalently the longitude 2α on the Poincaré sphere as shown on figure 2. The nanorod orientation $\theta \in [-\theta_{circ}, \theta_{circ}]$ defines the polarization ellipticity or equivalently the latitude on the Poincaré sphere according to a non trivial mapping $f(\theta) \approx \frac{90°}{\theta_{circ}}\theta$.

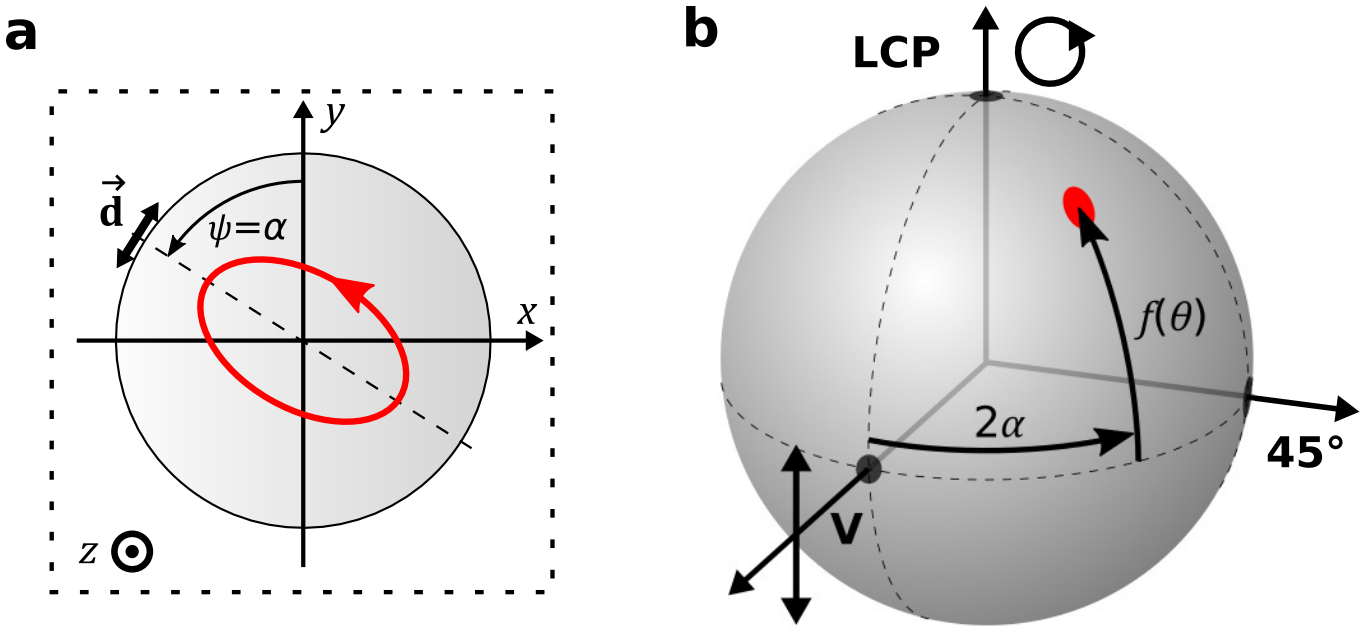

FIG. 2. **Mapping between dipole geometry and emitted polarization**. **(a)** Cut of the nanofiber. The azimuth of the dipole α defines the orientation of the polarization ellipse $\psi = \alpha$. **(b)** Poincaré sphere: a dipole with geometrical parameters (α, θ) gives rise to a guided polarization represented by a point with coordinate $(2\alpha, f(\theta))$ on the Poincaré sphere. V, 45° and LCP represent vertically linearly, linearly at $\psi = 45°$ and left-circularly polarized light respectively.

III. EXPERIMENT

A. Polarization measurement

Direct measurement of the polarization, i.e. determination of the Stokes parameters in the nanofiber region is hard to implement and we rather choose to measure the polarization state after light exits from one end of the fiber. While light propagates in the transition region, the adiabatic tapering enables almost perfect conversion from the fundamental mode of the nanofiber to the LP_{01} mode of the standard fiber. The polarization however is not maintained in practice, because of the significant birefringence in fibers. In order to still map the hybrid mode basis onto an accessible paraxial mode basis, we use a uniaxial birefringent plate mounted in the form of a Bereck compensator to compensate the birefringence effect of the fiber (see Appendix C).

B. Nanorods as linear dipoles

In our experiment, we use single gold nanorods that, under suitable illumination, behave as dipole scatterers with dipole orientations along the rods longitudinal axes. The deposition of a single nanorod on the nanofiber surface is performed by touching it with a small droplet of a commercial colloidal particle dispersion (Nanocomposix); this technique has an accuracy of a few hundred microns in the position of the particles along the nanofiber. The nanorods were chosen so that their longitudinal surface plasmon resonance (LSPR) matches our laser wavelength of 637 nm when deposited on the nanofiber. We hence work with nanorods of average aspect ratio of 2.6 yielding a LSPR centered around our working wavelength and with a size of 17 ± 1 nm in diameter and 45 ± 6 nm in length, considered small compared to the nanofiber geometry.

We model a nanorod as an anisotropic scatterer on which an exciting electric field $\mathbf{E}_{exc} = (E_L, E_T)$ induces a dipole moment $\mathbf{p} = (\alpha_L E_L, \alpha_T E_T)$ where α_L and α_T are the longitudinal and transverse polarizabilities of the rod, respectively. Close to the LSPR, $\mathrm{Im}(\alpha_L) \gg \mathrm{Im}(\alpha_T)$ and the transverse component of the dipole moment is strongly suppressed compared to the longitudinal component. We can hence suppose that, as long as the excitation field does not oscillate too perpendicularly with respect to the rod, in which case $\alpha_L E_L$ might be comparable to $\alpha_T E_T$, the dipole is induced along the nanorod.

To verify this crucial assumption experimentally, we rotated the excitation polarization while monitoring the power scattered by the nanorod into the nanofiber. We observed a sinusoidal dependence corresponding to a Malus law as shown in figure 3. The beam polarization angle for which the scattered signal is maximum is referred to as χ_{max}. In contrast to the collected power into the nanofiber, the guided polarization is almost unchanged when turning the excitation polarization. This validates the assumption that the dipole tends to align along the rod, independently of the excitation polarization. In the following experiments, we will always maximise the scattered signal by adjusting the beam polarization orientation to the value χ_{max} prior to acquiring the guided polarization state. The intrinsic diffusion of the excitation beam by the bare nanofiber is lower than 0.5 % of the overall scattered signal and can hence be neglected.

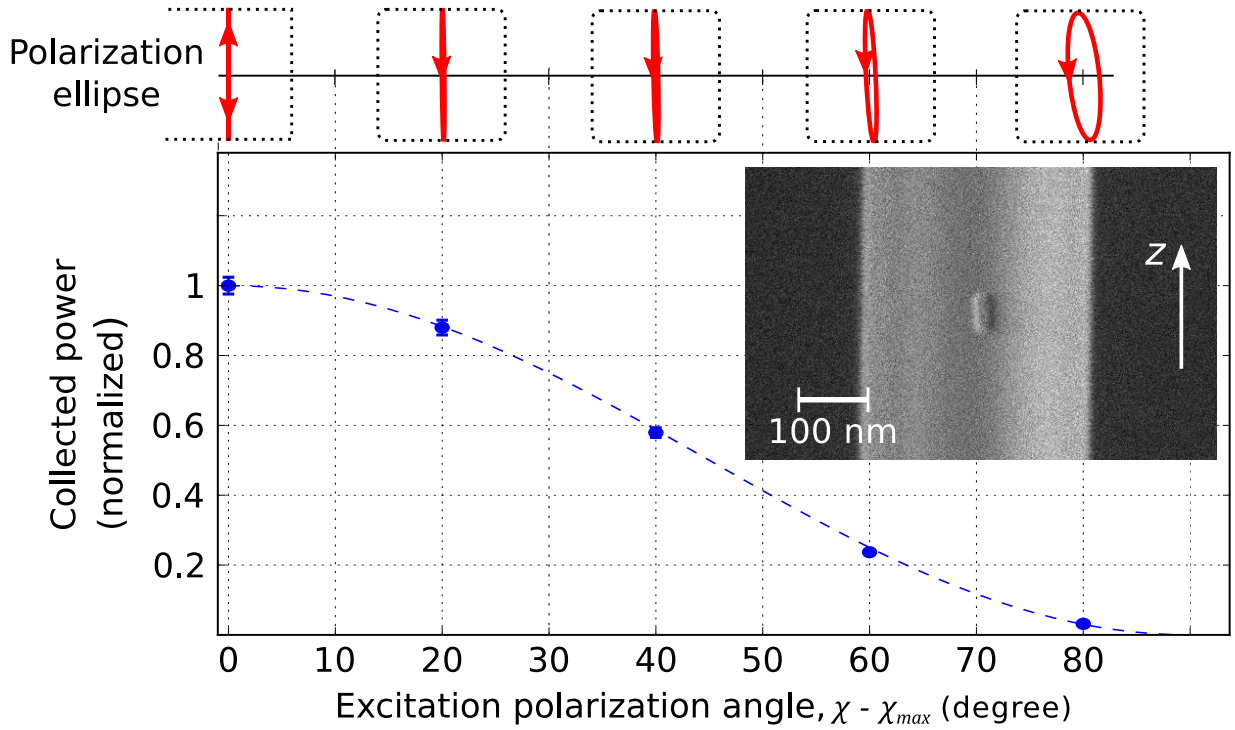

FIG. 3. **Nanorod optical response to rotating linear polarization excitation**. The lower graph represents the normalised collected power in the nanofiber as the excitation polarization angle χ rotates over 80°, starting at $\chi = \chi_{max}$ for which the scattered signal is maximum. The measured collected power is fitted to a Malus law. **Inset:** SEM image of the measured nanorod on the nanofiber. The upper plots represent the measured polarization ellipses for different excitation polarization angles. The guided polarization is almost independent of χ which constitutes a consistency check of our assumption that the dipole tends to form along the rod.

C. Experimental procedure

The experimental demonstration of the dependence between the nanorod geometry and the polarization of the guided light requires an ensemble of nanorods with various different positions and orientations. The experimental procedure is the following: (1) We deposit a first particle, (2) we compensate the birefringence of the fiber portion between the particle and the detection system, (3) we align the excitation polarization along the nanorod and (4) we record the guided polarization state. Next to the first particle, we then deposit a second particle and iterate the experimental procedure for the second particle. After that, we deposit a third particle and so on.

Since they are several particles on the same nanofiber, the light scattered by the nanorod under investigation and guided through the nanofiber towards the detection system could be scattered by the other particles, which could alter the polarization outcome. To prevent this issue, each new particle is deposited on the nanofiber between the previously deposited one and the detection system. This ensures that the light emitted by the last deposited nanorod encounters no obstacles when guided towards the detection system. A special care is also dedicated to have sufficient space between the different particles in order for the excitation beam to address nanorods individually. We also record the exact relative positions of the particles with respect to each other. This is meant to facilitate the finding of the nanorods when we ultimately observe the nanofiber with a SEM.

On the SEM, we identify the various depositions, disregard the clusters or the rods with odd shape to record only the azimuth α and the orientation θ of *proper* single nanorods. The orientation is determined from analysing SEM images as the one shown in the inset of figure 3. From this specific image, we extracted $\theta = 5 \pm 3°$. The uncertainty associated to the orientation is typically around a few degrees and is mainly due to the quality of the SEM images. We note that experimentally, we never observed rods with orientation $|\theta| \gtrsim 60°$ which we understand as the tendency for the nanorod to maximise its contact surface with the nanofiber.

D. Results & discussion

In our model of a linear dipole coupled to nanofiber modes, we predicted that the dipole orientation determines the polarization ellipticity. In order to express this dependence and compare our measurement to the model, we consider the normalised Stokes parameter S_3 as a function of the dipole/nanorod orientation θ as shown in figure 4a. S_3 ranges from -1 to 1 and provides us immediate information on the *degree of circular polarization* – defined as $|S_3|$ – and on the sense of circulation of the electric field in the transverse plane, related to the sign of S_3 (see Appendix D for a discussion of the uncertainties associated to the measured Stokes parameters). The figure also shows the measured corresponding polarization ellipses for five characteristic nanorods, the orientation of which varies from $-40°$ to $+46°$. As input parameters for the model, we took the average nanofiber diameter extracted from SEM images ($2a = 305 \pm 7$ nm), the working wavelength of 637 nm, 1.457 and 1.000 for the refractive index of silica and air respectively and we assumed 9 nm, which corresponds to the radius of a nanorod for the distance of the dipole to the nanofiber surface.

Our measurements of S_3 fit well our dipole model and present the characteristic behaviour presented above namely that, in the range $|\theta| \lesssim \theta_{circ}$, the degree of circular polarization grows with $|\theta|$ as the two components in (3) reach comparable amplitude. The case of circular polarization is expected at $\theta_{circ} = \pm 43°$ and experimentally, we observed almost purely circularly polarized light for a nanorod oriented at $\theta = 46 \pm 3°$. In contrast, nanorods nearly aligned along the nanofiber (small θ) induce a low degree of circular polarization and hence a narrow polarization ellipse. We also notice that the measured handedness of the polarization fits to our model as positive (negative) θ gives rise to counter-clockwise (clockwise) circulation of the electric field in the transverse plane.

We now consider the relation between the azimuthal position α of the nanorod and the polarization ellipse orientation ψ. This is easily observable for rods giving rise to narrow polarization ellipses, i.e. for which the orientation θ forms a small angle with the nanofiber. We hence consider five rods with orientations θ lying between $-20°$ and $20°$. Figure 4b shows the measured ellipse orientations as a function of the nanorod azimuth. The measured orientations of the polarization ellipses tend to follow the azimuthal positions of the nanorods.

Thus our experiments show that the measured polarization states as a function of the orientation and position of the nanorod are in good agreement with our linear dipole model. This constitutes an experimental demonstration that this system can generate all possible polarization states.

This realisation opens the possibilities for polarization control of single photon emitters coupled to nanofibers. Single photon sources with fully controllable polarization are of crucial importance for quantum cryptography protocols and a device based on our prototype can fulfil the requirements for this major application.

Indeed, the coupling of single photon sources with nanofibers has been reported [13, 18], as well as the polarized single photon emission of colloidal quantum dots [19, 20]. Additionally, orientation of nanoparticules has been achieved using optical tweezers [21].

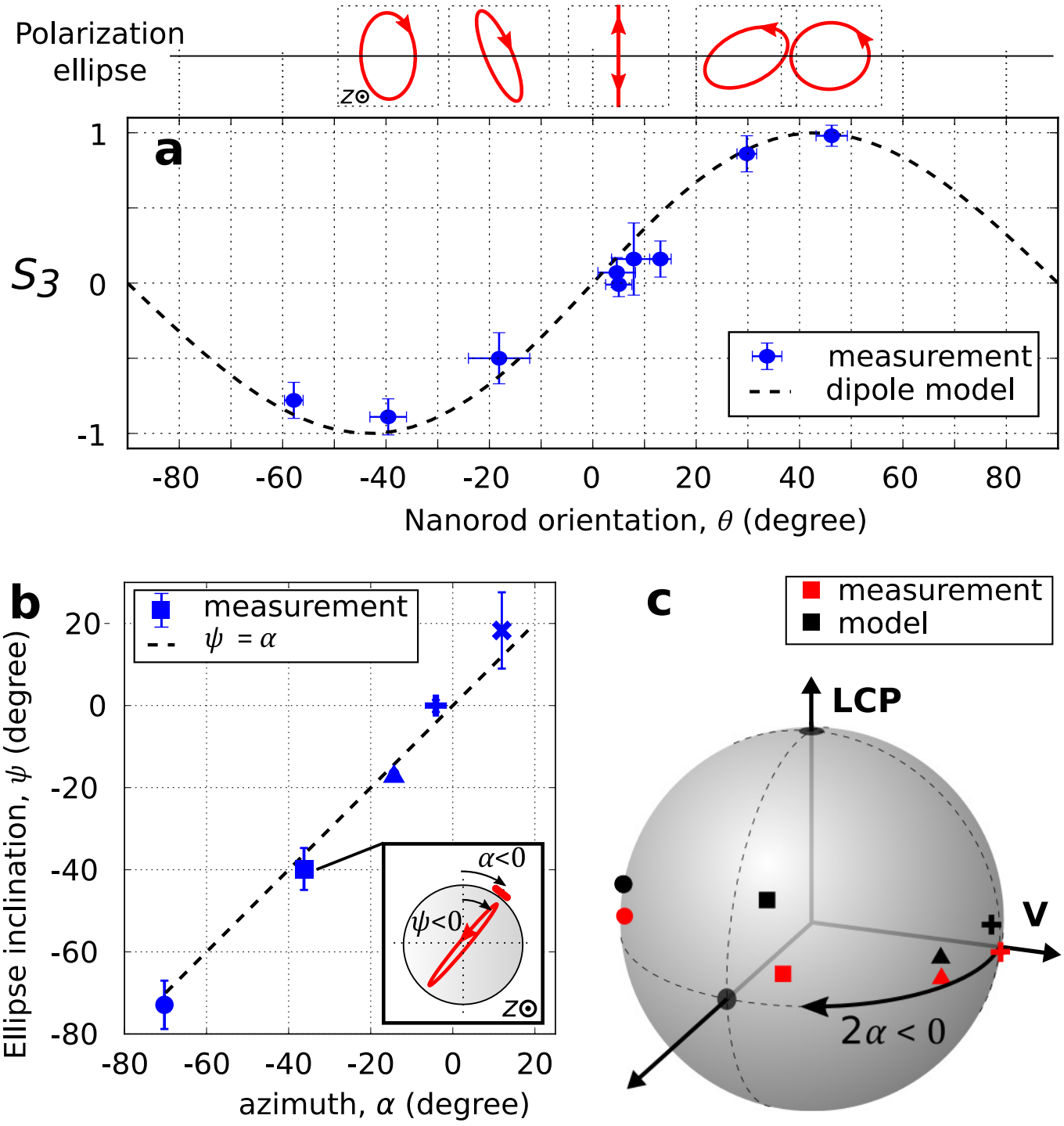

FIG. 4. **Measured state of polarization as a function of the orientation θ and azimuth α of the nanorod.** **(a)** Ellipticity as a function of θ. Graph : measured Stokes parameter S_3 for 9 different nanorods compared to the expected dipole model. We plot the measured polarization ellipse for characteristic nanorods. **(b)** Measured ellipse orientation ψ for 5 nanorods with different azimuth. The inset represents a cut of the nanofiber showing the azimuth of a specific nanorod and the associated polarization ellipse. **(c)** Poincaré sphere representation of the measured polarization for 4 nanorods from **(b)**.

Our results bring the last step for the realisation of a potential device with tunable polarization by showing the direct mapping between the spatial degrees of freedom of the source and the photon polarization.

Combining this mapping with an optical trapping and alignment technique [22], it is therefore possible to align the emitter to a desired orientation by sending inside the nanofiber a tweezer beam with a controlled polarization during the deposition procedure [22, 23]. Finally, once the emitter is correctly aligned, the same mapping (but in the reciprocal way) guarantees the desired polarization at the output of the fiber, as shown previously.

IV. CONCLUSION

In conclusion, we used gold nanorods deposited on a nanofiber to demonstrate that a linear dipole can radiate elliptically polarized light when coupled to spin-momentum locked modes. We showed that this system can, in principle, generate all possible polarization states. The azimuth position of the rod controls the inclination of the polarization ellipse while its orientation with respect to the nanofiber defines the ellipticity. This constitutes a demonstration of the mapping between purely geometrical degrees of freedom of a light source and polarization states. This system opens a new way for controlling the polarization of light sources at the nanoscale without involving birefringent components or magnetic fields.

V. ACKNOWLEDGMENTS

The authors thanks Clément Sayrin for his helpful suggestions throughout this work, Imène Estève for her decisive support on the SEM platform and Sébastien Bidault for fruitful discussions. This work is supported by the Emergence program from Ville de Paris, by PSL Research University in the framework of the project COSINE and by the Cai Yuanpei program.

Appendix A: Hybrid modes

An optical nanofiber in the single mode regime only guides the fundamental mode associated to a unique propagation constant β where $n_1 k > \beta > n_2 k$, k is the wavenumber of light in vacuum, n_1 and n_2 are the refractive indices of the fiber and surrounding medium respectively. General expressions for the electric field of the fundamental mode can be found in [4]. We consider here the orthogonal basis of quasi-linearly polarized modes along x' and y' where we use the cartesian coordinate system $(x'y'z)$ introduced in the main text. For the region outside of the nanofiber ($r > a$) and light propagating in the positive $z-$direction, the complex enveloped of the modes are:

$$\mathbf{HE}_{11,x'} = N\frac{J_1(ha)}{K_1(qa)}\begin{pmatrix} \frac{\beta}{2q}\left[(1-s)K_0(qr)+(1+s)K_2(qr)\cos(2\varphi)\right] \\ \frac{\beta}{2q}(1+s)K_2(qr)\sin(2\varphi) \\ iK_1(qr)\cos(\varphi)\end{pmatrix} \tag{A1}$$

$$\mathbf{HE}_{11,y'} = N\frac{J_1(ha)}{K_1(qa)}\begin{pmatrix} \frac{\beta}{2q}(1+s)K_2(qr)\sin(2\varphi) \\ \frac{\beta}{2q}\left[(1-s)K_0(qr)-(1+s)K_2(qr)\cos(2\varphi)\right] \\ iK_1(qr)\sin(\varphi)\end{pmatrix} \tag{A2}$$

where r, φ are the polar coordinates in the $x'y'-$plane. N is a normalization constant, a is the nanofiber radius,

$$s = [(qa)^{-2} + (ha)^{-2}]/[J_1'(ha)/(haJ_1(ha)) + K_1'(qa)/(qaK_1(qa))],$$

$h = \sqrt{n_1^2k^2 - \beta^2}$, $q = \sqrt{\beta^2 - n_2^2k^2}$, J_n, K_n are the Bessel functions of the first kind and the modified Bessel functions of the second kind respectively, and the prime stands for the derivative.

Appendix B: Modal amplitudes for a linear dipole coupled to $\mathbf{HE}_{11}$

At the dipole (nanorod) position ($r = \rho, \varphi = \pi/2$), the hybrid modes take the value:

$$\mathbf{HE}_{11,x'}(\rho, \pi/2) = (\epsilon_1, 0, 0) \tag{B1}$$

$$\mathbf{HE}_{11,y'}(\rho,\pi/2) = (0,\epsilon_2,i\epsilon_3) \tag{B2}$$

where $\epsilon_1 = N\frac{J_1(ha)}{K_1(qa)}\frac{\beta}{2q}\left[(1-s)K_0(q\rho)-(1+s)K_2(q\rho)\right]$, $\epsilon_2 = N\frac{J_1(ha)}{K_1(qa)}\frac{\beta}{2q}\left[(1-s)K_0(q\rho)+(1+s)K_2(q\rho)\right]$, $\epsilon_3 = N\frac{J_1(ha)}{K_1(qa)}K_1(q\rho)$ and ρ is the radial position of the dipole. The dot products between the dipole moment $\mathbf{d}^* = d\left[\sin\theta,\ 0,\ \cos\theta\right]$ and the hybrid modes read:

$$A \overset{def}{=} \mathbf{d}^* \cdot \mathbf{HE}_{11,x'}(\rho,\pi/2) = d\epsilon_1 \sin\theta \tag{B3}$$

$$B \overset{def}{=} \mathbf{d}^* \cdot \mathbf{HE}_{11,y'}(\rho,\pi/2) = i\ d\epsilon_3 \cos\theta. \tag{B4}$$

where d is real. Emission of quasi-circularly polarized light occurs when $|A| = |B|$ which leads to:

$$\epsilon_1 \sin\theta = \epsilon_3 \cos\theta. \tag{B5}$$

This can be numerically solved and leads to $\theta_{circ} = \pm 43°$ for our experimental parameters: $\rho = a+9$ nm, $2a = 305$ nm, $\lambda = 637$ nm, $n_1 = 1.457$ and $n_2 = 1.000$.

At the output of the fiber, i.e. at the detection system, the normalised Stokes parameters are given by:

$$\begin{aligned} S_1 &= (|A|^2 - |B|^2)/S_0 \\ S_2 &= 2\ \mathrm{Re}(A^*B)/S_0 \\ S_3 &= 2\ \mathrm{Im}(A^*B)/S_0 \end{aligned} \tag{B6}$$

where $S_0 = |A|^2 + |B|^2$. The degree of polarization is $\sqrt{S_1^2+S_2^2+S_3^2}$, it is equal to 1 for purely polarized light. In our experiment, we measured an average degree of polarization of 0.98 ± 0.01 for the guided light emitted by the nanorod. S_1 and S_2 are dependent of the coordinate system whereas S_3 is rotation invariant. In the coordinate system $(x'y')$ introduced in the main text, $S_2 = 0$.

In the main text, we showed that a dipole with geometrical parameters (α,θ) gives rise to a guided polarization represented by a point with coordinate $(2\alpha, f(\theta))$ on the Poincaré sphere. For purely polarized light and $\theta \in [-\theta_{circ},\theta_{circ}]$, we have:

$$\begin{aligned} f(\theta) &= \arcsin S_3 \\ &\approx \frac{90°}{\theta_{circ}}\theta \end{aligned} \tag{B7}$$

where the error made with the approximation does not exceed 3% in typical experimental conditions.

Appendix C: Birefringence compensation

In order to find the adjustment of the Berek compensator that compensates the birefringence introduced by the fiber setup, we observe the Rayleigh scattering [24] in the nanofiber region when light is sent from the polarimeter toward the nanofiber, through the compensator and the fiber setup. The light scattering is assumed to originate from imperfections in the nanofiber. Because Rayleigh scattering preserves the polarization, its analysis can give information on the polarization of the propagating fundamental mode in the nanofiber. Especially, Rayleigh scattering enables to align the polarization in the nanofiber quasi-linearly along the axis of observation or orthogonal to it. Since we can recognize an orthogonal hybrid basis in the nanofiber region, the compensation procedure consists in finding the Berek compensator adjustment that map the orthogonal polarization basis at the polarimeter location with the hybrid basis in the nanofiber.

Appendix D: Uncertainty on the measured Stokes parameters

The measurement of the state of polarization of the guided light emitted by the nanorod is subject to random errors and systematic errors.

1. Random errors

Random errors are dominated by fluctuations of the power scattered by the nanorod, principally due to vibrations of the nanofiber holding the nanorod in the focus of the excitation laser beam and, to a smaller extent, to intrinsic laser intensity fluctuations. These power fluctuations introduce a dispersion on the measured normalised Stokes parameters as low as $\sigma = 0.01$.

2. Systematic error

The uncertainty on the measured state of polarization of the light emitted by the nanorod is in fact largely dominated by a systematic error. It comes from the non-perfect birefringence compensation described above. Ideally, once the Berek compensator has been adjusted correctly, quasi-linearly polarized light in the nanofiber region should be mapped onto linearly polarized light at the polarimeter location. In practice, we observe a residual ellipticity, which implies a systematic error on the measured normalized Stokes parameters. Typical errors on the normalized Stokes parameters range from 0.01 to 0.24 with an average of 0.1.

[1] Oliver Benson, "Assembly of hybrid photonic architectures from nanophotonic constituents," Nature **480**, 193 – 199 (2011).
[2] Lukas Novotny and Niek van Hulst, "Antennas for light," Nature Photonics **5**, 83 – 90 (2011).
[3] Rui Guo, Manuel Decker, Frank Setzpfandt, Xin Gai, Duk-Yong Choi, Roman Kiselev, Arkadi Chipouline, Isabelle Staude, Thomas Pertsch, Dragomir N. Neshev, and Yuri S. Kivshar, "High–bit rate ultra-compact light routing with mode-selective on-chip nanoantennas," Science Advances **3** (2017), 10.1126/sciadv.1700007.
[4] Fam Le Kien, J.Q. Liang, K. Hakuta, and V.I. Balykin, "Field intensity distributions and polarization orientations in a vacuum-clad subwavelength-diameter optical fiber," Optics Communications **242**, 445 – 455 (2004).
[5] Todd Van Mechelen and Zubin Jacob, "Universal spin-momentum locking of evanescent waves," Optica **3**, 118–126 (2016).
[6] Peter Lodahl, Sahand Mahmoodian, Sren Stobbe, Arno Rauschenbeutel, Philipp Schneeweiss, Jrgen Volz, Hannes Pichler, and Peter Zoller, "Chiral quantum optics," Nature **541**, 473 – 480 (2017).
[7] Francisco J. Rodríguez-Fortuño, Giuseppe Marino, Pavel Ginzburg, Daniel O'Connor, Alejandro Martínez, Gregory A. Wurtz, and Anatoly V. Zayats, "Near-field interference for the unidirectional excitation of electromagnetic guided modes," Science **340**, 328–330 (2013).
[8] Jan Petersen, Jürgen Volz, and Arno Rauschenbeutel, "Chiral nanophotonic waveguide interface based on spin-orbit interaction of light," Science **346**, 67–71 (2014).
[9] Immo Söllner, Sahand Mahmoodian, Sofie Lindskov Hansen, Leonardo Midolo, Alisa Javadi, Gabija Kiršanskė, Tommaso Pregnolato, Haitham El-Ella, Eun Hye Lee, Jin Dong Song, Sren Stobbe, and Peter Lodahl, "Deterministic photonemitter coupling in chiral photonic circuits," Nature Nanotechnology **10**, 775–778 (2015).
[10] Clément Sayrin, Christian Junge, Rudolf Mitsch, Bernhard Albrecht, Danny O'Shea, Philipp Schneeweiss, Jürgen Volz, and Arno Rauschenbeutel, "Nanophotonic optical isolator controlled by the internal state of cold atoms," Phys. Rev. X **5**, 041036 (2015).
[11] Francisco J. Rodríguez-Fortuño, Daniel Puerto, Amadeu Griol, Laurent Bellieres, Javier Mart, and Alejandro Martínez, "Universal method for the synthesis of arbitrary polarization states radiated by a nanoantenna," Laser & Photonics Reviews **8**, L27–L31 (2014).
[12] Alba Espinosa-Soria, Francisco J. Rodríguez-Fortuño, Amadeu Griol, and Alejandro Martínez, "On-chip optimal stokes nanopolarimetry based on spinorbit interaction of light," Nano Letters **17**, 3139–3144 (2017).
[13] Ramachandrarao Yalla, Fam Le Kien, M. Morinaga, and K. Hakuta, "Efficient channeling of fluorescence photons from single quantum dots into guided modes of optical nanofiber," Phys. Rev. Lett. **109**, 063602 (2012).
[14] Mark Sadgrove, Masakazu Sugawara, Yasuyoshi Mitsumori, and Keiichi Edamatsu, "Polarization response and scaling law of chirality for a nanofibre optical interface," Scientific Reports **7** (2017), 10.1038/s41598-017-17133-3.
[15] J. E. Hoffman, S. Ravets, J. A. Grover, P. Solano, P. R. Kordell, J. D. Wong-Campos, L. A. Orozco, and S. L. Rolston, "Ultrahigh transmission optical nanofibers," AIP Advances **4**, 067124 (2014).
[16] Daniel Reitz and Arno Rauschenbeutel, "Nanofiber-based double-helix dipole trap for cold neutral atoms," Optics Communications **285**, 4705 – 4708 (2012), special Issue: Optical micro/nanofibers: Challenges and Opportunities.
[17] Allan W. Snyder and John D. Love, *Optical Waveguide Theory* (Chapman & Hall, 1983) Chap. 21.
[18] Lars Liebermeister, Fabian Petersen, Asmus v. Mnchow, Daniel Burchardt, Juliane Hermelbracht, Toshiyuki Tashima, Andreas W. Schell, Oliver Benson, Thomas Meinhardt, Anke Krueger, Ariane Stiebeiner, Arno Rauschenbeutel, Harald Weinfurter, and Markus Weber, "Tapered fiber coupling of single photons emitted by a deterministically positioned single nitrogen vacancy center," Applied Physics Letters **104**, 031101 (2014).
[19] Stefano Vezzoli, Mathieu Manceau, Godefroy Lemnager, Quentin Glorieux, Elisabeth Giacobino, Luigi Carbone, Massimo De Vittorio, and Alberto Bramati, "Exciton fine structure of cdse/cds nanocrystals determined by polarization microscopy at room temperature," ACS Nano **9**, 7992–8003 (2015).

[20] M. Manceau, S. Vezzoli, Q. Glorieux, F. Pisanello, E. Giacobino, L. Carbone, M. De Vittorio, and A. Bramati, "Effect of charging on cdse/cds dot-in-rods single-photon emission," Phys. Rev. B **90**, 035311 (2014).
[21] Onofrio M. Maragò, Philip H. Jones, Pietro G. Gucciardi, Giovanni Volpe, and Andrea C. Ferrari, "Optical trapping and manipulation of nanostructures," Nature Nanotechnology **8**, 807 819 (2013).
[22] Lianming Tong, Vladimir D. Miljković, and Mikael Käll, "Alignment, rotation, and spinning of single plasmonic nanoparticles and nanowires using polarization dependent optical forces," Nano Letters **10**, 268–273 (2010).
[23] Matthew Pelton, Mingzhao Liu, Hee Y. Kim, Glenna Smith, Philippe Guyot-Sionnest, and Norbert F. Scherer, "Optical trapping and alignment of single gold nanorods by using plasmon resonances," Opt. Lett. **31**, 2075–2077 (2006).
[24] E. Vetsch, S. T. Dawkins, R. Mitsch, D. Reitz, P. Schneeweiss, and A. Rauschenbeutel, "Nanofiber-based optical trapping of cold neutral atoms," IEEE Journal of Selected Topics in Quantum Electronics **18**, 1763–1770 (2012).